# Computer-aided detection of wall motion abnormalities in cardiac MRI

Suinesiaputra, A.

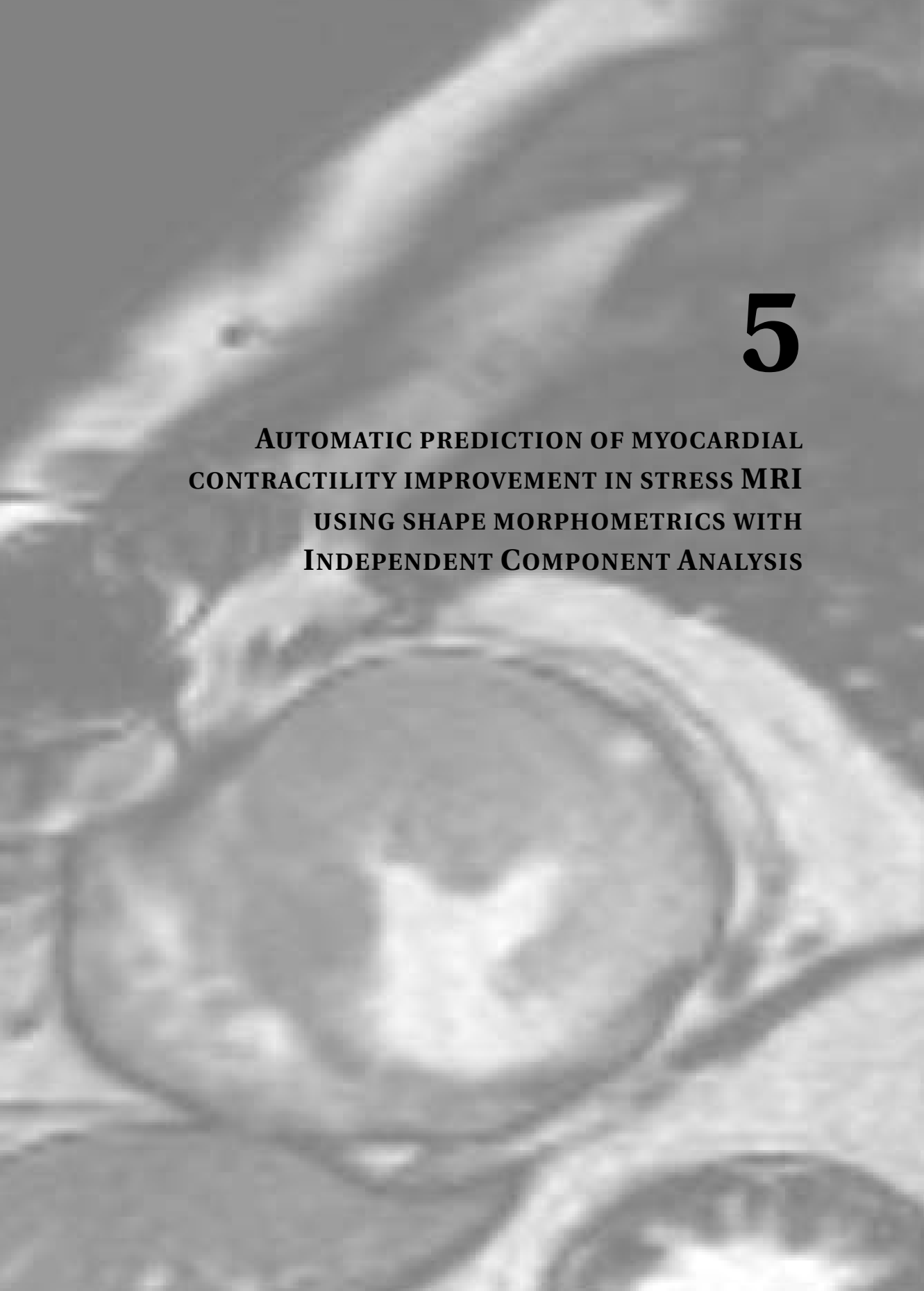

# 5

# AUTOMATIC PREDICTION OF MYOCARDIAL CONTRACTILITY IMPROVEMENT IN STRESS MRI USING SHAPE MORPHOMETRICS WITH INDEPENDENT COMPONENT ANALYSIS

**Abstract**

An important assessment in patients with ischaemic heart disease is whether myocardial contractility may improve after treatment. The prediction of myocardial contractility improvement is generally performed under physical or pharmalogical stress conditions. In this chapter, a technique to build a statistical model of healthy myocardial contraction using independent component analysis is presented. The model is applied for detecting regions with abnormal contraction in patients both during rest and stress.

This chapter was adapted from:
A. Suinesiaputra, A. F. Frangi, H. J. Lamb, J. H. C. Reiber, and B. P. F. Lelieveldt. Automatic prediction of myocardial contractility improvement in stress MRI using shape morphometrics with independent component analysis. In G. E. Christensen and M. Sonka, editors, *Information Processing in Medical Imaging*, volume 3565 of *Lecture Notes in Computer Science*, pages 321–332. Springer, 2005.

He deals the cards to find the answer.
The sacred geometry of chance.
The hidden law of probable outcome.
The numbers lead a dance.

Shape of My Heart
STING

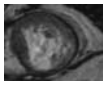



ISCHAEMIC heart disease is a major heart disease in the western world. Non-invasive diagnosis of ischaemia has been developed in recent years (see [1] for the survey of different imaging techniques). Among others, Magnetic Resonance Imaging (MRI) has attracted many clinicians due to its excellent spatial and temporal resolution, high-contrast of soft tissue, accurate and reproducible global and regional ventricular functions, flow and perfusion during rest and pharmacological stress, and the possibility of using paramagnetic contrast agent to enhance the intensity of myocardial infarction areas [2, 3].

One crucial assessment in ischaemic heart disease is to determine the presence of hibernating myocardium. This is a viable but dysfunctional myocardium, which may improve its function after treatment [1]. The prediction of improvement of myocardial contraction is only possible during physical or pharmacological stress [4]. Thus, the identification of dysfunctional myocardium that improves under stress is an important factor in the treatment of ischaemic heart disease.

Low-dose dobutamine stress MRI can be used to evaluate improvement of myocardial contraction in ischaemic patients [1, 5]. In this procedure, a low dose of dobutamine is administered prior to MR acquisition to produce stress images. Usually, visual comparison between the rest and stress cine images is performed for visual wall motion scoring. However, this visual assessment is very difficult and subjective, because differences between rest and stress motion may be very subtle.

The goal of this work is to develop a method to automatically detect subtle changes in cardiac contraction between rest and stress. In this chapter, further expansion of previously described work (see Chapter 4) on modeling the myocardial contraction of healthy hearts is presented [6]. A statistical contraction model is trained from myocardial contours in rest condition using Independent Component Analysis (ICA) to construct a set of locally selective basis functions. Analysis is performed by projecting patient shapes onto this basis, and in Chapter 4, this model is used to automatically detect and localize abnormal cardiac contraction in rest. The main improvements of this chapter are twofold:

- The ICA modeling framework is improved by adopting a principled way of selecting the optimal number of components, and introducing kernel density estimation to describe the model parameter distributions for normal contraction.

- The rest-stress comparison framework is introduced. By comparing the projection parameters in rest and stress conditions, one can assess which regions of myocardium show contractility improvement under stress, and therefore may be viable.

This chapter is organized as follows. Section 5.1 describes the statistical modeling of normal contraction by using ICA. In Section 5.2, we present the qualitative prediction results of myocardial viability in stress condition, followed by a discussion in Section 5.3.

## 5.1 Methodology

ICA is originally used for finding source signals from a mixture of unknown signals without prior knowledge other than the number of sources [7]. There have been some studies to use ICA in machine learning for feature extraction [8], face recognition [9] and classification [10]. Previously, a statistical model to detect regional abnormalities from infarct patients using ICA has been reported [6]. The advantage of using ICA over other decompositions is the fact that ICA yields locally independent detectors that can be used to determine regional shape abnormalities, whereas PCA yields global shape variations that influence the entire shape.

ICA is a linear generative model, where every training shape can be approximated by a linear combination of its components. Let $\mathbf{x} = (x_1, y_1, \ldots, x_m, y_m)^T$ be a shape vector, consisting of $m$ pairs of $(x, y)$ coordinates of landmark points. The linear generative model is formulated as follows:

$$\mathbf{x} \approx \bar{\mathbf{x}} + \Phi \mathbf{b} \ . \tag{5.1}$$

The matrix $\Phi \in \mathbb{R}^{2m \times p}$ defines the independent components (ICs) and $\mathbf{b} \in \mathbb{R}^p$ is the weight coefficient vector. The mean shape, $\bar{\mathbf{x}}$, is defined by

$$\bar{\mathbf{x}} = \frac{1}{n} \sum_{i=1}^{n} \mathbf{x}_i \ . \tag{5.2}$$

where $n$ is the number of shapes and $p$ is the number of retained components.

The goal of ICA is to find a matrix, $\Psi$, such that

$$\mathbf{b} = \Psi (\mathbf{x} - \bar{\mathbf{x}}) \tag{5.3}$$

with a constraint that columns of $\Psi$ correspond to statistically independent directions. Thus the independent components are given by $\Phi = \Psi^{-1}$. The matrix $\Psi$ is estimated by a suitable optimisation algorithm (see [11] for survey of ICA).

### 5.1.1 Modeling contraction of healthy myocardium

The observed shapes are taken from LV epi- and endocardial contours from short-axis MR images. To model the contractility pattern, contours for each subject are combined serially into one shape vector in the following order: endocardial contour at *end-diastole* (ED), epicardial contour at ED, endocardial contour at *end-systole* (ES) and epicardial contour at ES.

Prior to shape modeling, Procrustes shape alignment on the four contours at once was performed as a pre-processing step to eliminate global shape differences in pose and scale between the samples [12]. Mean shape of the training shapes after the alignment is shown in Figure 5.1.

Since the improvement of motion contraction from rest to stress is the main issue, *centerline* points, i.e. points in the the middle between epi- and endocardial contours, were used in ICA. The centerline method has already been used in a rest and stress study to diagnose coronary artery disease [13]. Figure 5.1(c) shows the centerline points from the mean shape.

Four examples of independent components from the centerline model are shown in Figure 5.2. The independent components (ICs) show an interesting and important property where shape variations are local. In the diagnosis, these shape variations are used as detectors to determine local shape abnormalities, i.e. regions with abnormal contraction.

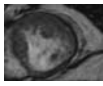



### 5.1.2 Optimal number of independent components

If the number of source signals in ICA is not known a priori, the number of components needs to be determined. Many methods have been proposed to estimate this parameter, for instance, by using mutual information [14], neural networks [15], a Bayesian approach [16], and clustering techniques [17]. Though these approaches are different, the basic idea is to determine which are "weak" and "strong" independent components. Strong ICs represents reliable components.

For this study, the clustering technique proposed by Himberg et. al. [17][1] is adopted. This approach selects reliable ICs from a number of different realizations of ICs with different initializations. The selection is performed by clustering the resulting ICs. This approach was selected because of stochastic nature of computing ICs with the FastICA [7], the most popular and robust ICA algorithm that we used in this study.

After each trial, each IC is represented as a single point in a source space. The reliability of the estimated ICs can be analyzed by looking at the spread of the obtained ICs. The ICs form clusters in the source space, and the more compact and isolated the cluster of an IC, the more reliable is the IC (see Figure 5.3(b)). To measure the reliability of a cluster,

[1] The implementation is known as the Icasso package [17].

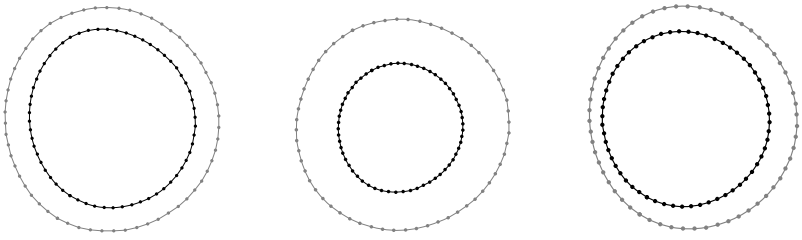

(a) aligned shapes at ED (b) aligned shapes at ES (c) centerline points

FIGURE 5.1: Mean shape of the aligned training shapes.

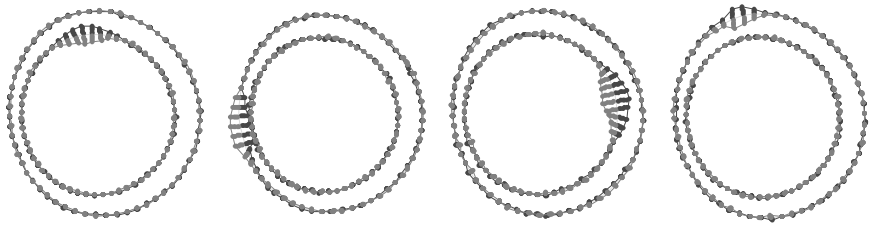

FIGURE 5.2: Four examples of independent components from model. Dots are shape variations, where the maximum is $\pm 3\sigma$ (standard deviation). The inner and outer contours are ES and ED centerline points, respectively.

an agglomerative hierarchical clustering is performed. A quality index of an IC, $I_q$, that reflects the compactness and isolating of a cluster, is defined as

$$I_q(C_m) = \frac{1}{|C_m|^2} \sum_{i,j \in C_m} \sigma_{ij} - \frac{1}{|C_m||C_{-m}|} \sum_{i \in C_m} \sum_{j \in C_{-m}} \sigma_{ij} \tag{5.4}$$

where $C_m$ and $C_{-m}$ are the set of indices that belong and do not belong to the $m$-cluster, respectively. The $\sigma_{ij}$ is a similarity measurement between $i$-th and $j$-th IC using their mutual correlation coefficient $r_{ij}$, i.e.

$$\sigma_{ij} = |r_{ij}| \,. \tag{5.5}$$

The value of $I_q$ increases when $C_m$ becomes more compact and isolated.

Another measurement to indicate reliable ICs in the clustering technique is the R-index, $I_R$

$$I_R = \frac{1}{L} \sum_{m=1}^{L} \frac{S_m^{\text{in}}}{S_m^{\text{ex}}} \tag{5.6}$$

where

$$\begin{aligned} S_m^{\text{in}} &= \frac{1}{|C_m|^2} \sum_{i,j \in C_m} d_{ij} \\ S_m^{\text{ex}} &= \min_{m' \neq m} \frac{1}{|C_m||C_{m'}|} \sum_{i \in C_m} \sum_{j \in C_{m'}} d_{ij} \quad . \end{aligned}$$

$d_{ij}$ is a dissimilarity measurement, defined as $d_{ij} = 1 - \sigma_{ij}$. The R-index is basically a ratio between the *within-cluster* and *between-cluster* ratio.

The R-index and the quality index indicate improved clustering in opposite directions. The optimal value for the number of computed ICs is when $I_q$ is large and $I_R$ is small. The plot of $I_q$ and $I_R$ for our study is shown in Figure 5.3(a).

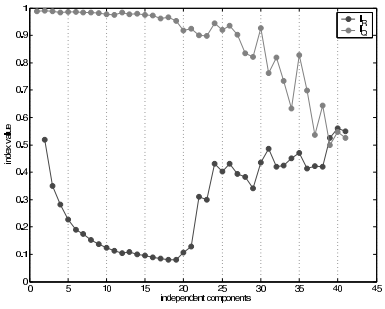


(a) The quality and the R-index.

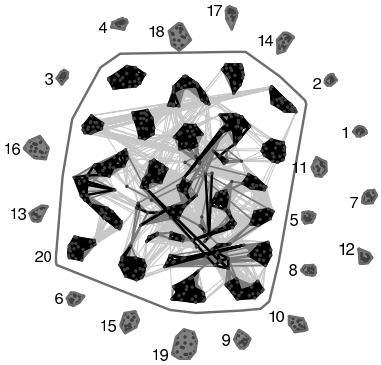


(b) Cluster visualization

FIGURE 5.3: $I_q$ and $I_R$ plot and the visualization of the estimated ICs in the cluster space. In the right figure, clusters are indicated by convex hull borders. Grey lines connect estimates whose similarity is larger than a threshold, the darker the line the stronger the similarity. Labels correspond to independent components. Notice that reliable components are compact and isolated.

The visualization of IC clusters is shown in Figure 5.3(b). Each estimated IC is represented as a single point in the cluster space. Reliable ICs form compact and isolated clusters. In Figure 5.3(b), ICs number 1 until 19 are reliable, whereas the remaining ICs are not reliable (they are glued together as one cluster number 20). The gray lines in Figure 5.3(b) denote dependencies at some threshold values between clusters.

### 5.1.3 Density estimation of coefficient values from the ICA model

In (5.1), the **b** vector represents the projection of a shape **X** onto the IC basis $\Phi$. The **b** vector contains coefficient values for the model that are needed to approximate the shape **X** from the IC basis. If the shape of **X** is similar to the shapes that construct the IC basis, then the coefficient values are within the distribution of the **b** vector of the model. On the contrary, the coefficient values are outside of the distribution. Hence, the detection of abnormal shapes becomes a problem of estimating the probability density function of the model coefficient values.

Since the ICA model is built from $n$ training shapes, (5.1) can be simply reformulated in matrix form as:

$$\mathbf{X} = \bar{\mathbf{x}} \cdot \mathbf{1}^T + \Phi \mathbf{B} \ . \tag{5.7}$$

The probability density function is estimated from of each column in matrix **B**. Figure 5.4 shows the distribution of each coefficient value from the healthy heart contraction for each IC (column of **B**), with an example of a projected patient shape.

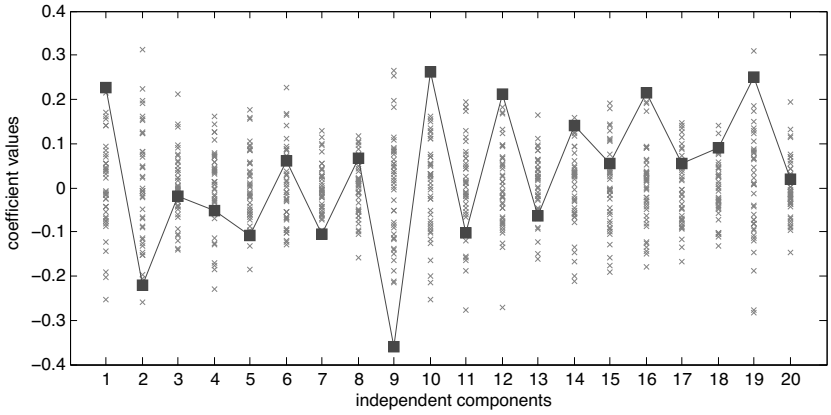


FIGURE 5.4: Distribution of coefficient values of healthy heart contraction (crosses) with an example of coefficient values from the projected shape of a patient (solid lines).

In ICA, components are sought to be statistically independent. This is achieved by finding the direction of components that maximizes the nongaussianity. The result is an independent basis which is non-orthogonal. The components have non-gaussian distribution, or at most only one with a gaussian distribution [7]. By statistical independency assumption, the multivariate density estimation of the matrix **B** can be simplified into univariate density estimation. Therefore, the probability density function on each of IC can be estimated separately.

To estimate the density function, a non-parametric kernel density estimation is applied on each of the independent component [19]. The kernel density estimation for the $j$-th component is defined by

$$\hat{f}_j(x) = \frac{1}{nh} \sum_{i=1}^{n} K\left(\frac{x - \mathbf{B}_{i,j}}{h}\right) \tag{5.8}$$

where $\mathbf{B}_{i,j}$ is the coefficient values in the matrix **B** in (5.7) at $j$-th independent component. The bandwidth $h$ and the kernel function $K(u)$ are the two parameters of the kernel density estimation method.

Gaussian function is used for the kernel function, i.e.,

$$K(u) = \frac{1}{\sqrt{2\pi}} \exp\left(-\frac{u^2}{2}\right) \tag{5.9}$$

Note that the choice of kernel function is not really critical for the kernel density estimation, but rather for the choice of bandwidth [19].

The bandwidth $h$ controls the amount of smoothing. A small difference in setting $h$ can yield a big difference in the probability function. We applied the Sheather-Jones solve-

the-plugin method level 2 to estimate the optimal bandwidth [20]. This solve-the-plugin method solves an unknown functional parameter in the optimal bandwidth equation directly from the sample distribution.

After estimating the probability density function $\hat{f}_j(x)$ for each IC, the quantification of abnormalities is straightforward. A probability map of being abnormal for each IC is defined as

$$\hat{p}_j(x) = 1 - \hat{f}_j(x) \ . \tag{5.10}$$

A threshold value $\rho$ is defined to determine the abnormality. Coefficient values that fall below that threshold are considered to be normal.

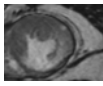



## 5.2 Experimental Results

### 5.2.1 Model construction

An ICA model of healthy myocardial heart contraction was built by selecting epicardial and endocardial borders at ED and ES phases from 42 healthy volunteers. The mid ventricular level from short-axis MRI was taken from each subject. Contours were drawn manually by an expert and used 60 landmark points per contour, defined by equi-angular sampling from the center of the myocardium. To ensure point correspondence between shapes, a fixed reference point was defined at the intersection between left and right ventricle.

ICA was performed using FastICA algorithm [7], implemented in Matlab (Matlab v6.5, The Mathworks, Natick, MA, USA). FastICA uses an optimization algorithm to maximize the *non-Gaussianity* of each component's direction to ensure that components are statistically independent between each other. The nonlinearity objective function used in the optimization process is $g(y) = 3y^2$ (or *pow*) and with symmetric orthogonalization. The number of independent components was determined following Himberg's approach [17], as has been described in Section 5.1.2. The number of trials was set to 20.

### 5.2.2 Qualitative prediction results of contractility improvement

To qualitatively evaluate the prediction of myocardial contractility improvement under stress, MR data of six representative patients with acute myocardial infarction were selected. The threshold value, $\rho$, separating abnormal from normal coefficient values, is empirically defined as 0.8. Figure 5.5 and Figure 5.6 show the visualization of abnormal regions in rest and stress for the six patients.

The left and middle figures are the quantification of abnormal contraction regions from the method in rest and stress, respectively. Regions with abnormal contraction are shown with dark colors inside of the myocardium. The darker the color, the more abnormal the regional motion. Thus regions with contractility improvement are visible by the decreasing amount of darkness from rest to stress in the corresponding regions.

Each of the abnormal regions has a corresponding abnormal independent component that is shown as bar plot at the right figure, given as the probability value of being

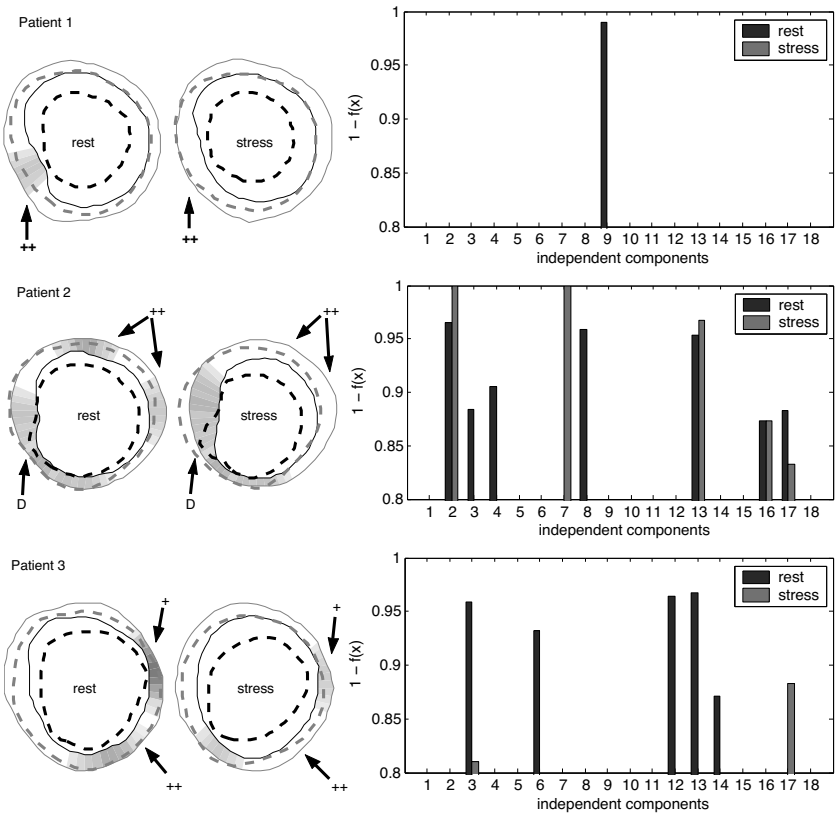


FIGURE 5.5: Qualitative prediction results of myocardial contractility improvement from Patients 1, 2, and 3. The leftmost and middle figures are quantification of abnormal regions from rest and stress respectively. ED and ES contours are drawn in solid and dashed lines respectively, to visualize contraction of the heart. The right most figure shows the abnormal independent components.

abnormal. Contractility improvement of an IC is shown as a decreasing amount of the probability value from rest to stress.

Contraction motion is visualized with the ED (solid lines) & ES (dashed lines) contours that are plotted together. It can be seen from Figure 5.5 and Figure 5.6 that regions with abnormal contraction motion correspond visually with the dark areas.

Arrows in Figure 5.5 and Figure 5.6 point to some interesting regions in each patient. If contraction in a region is improved, then the arrow is marked with '+' sign (Patient 3 and 5). Regions with a lot of contractility improvement, where they are detected as normal in stress, are marked with '++' sign. These are seen at Patient 1, 2, 3, 4 and 6.

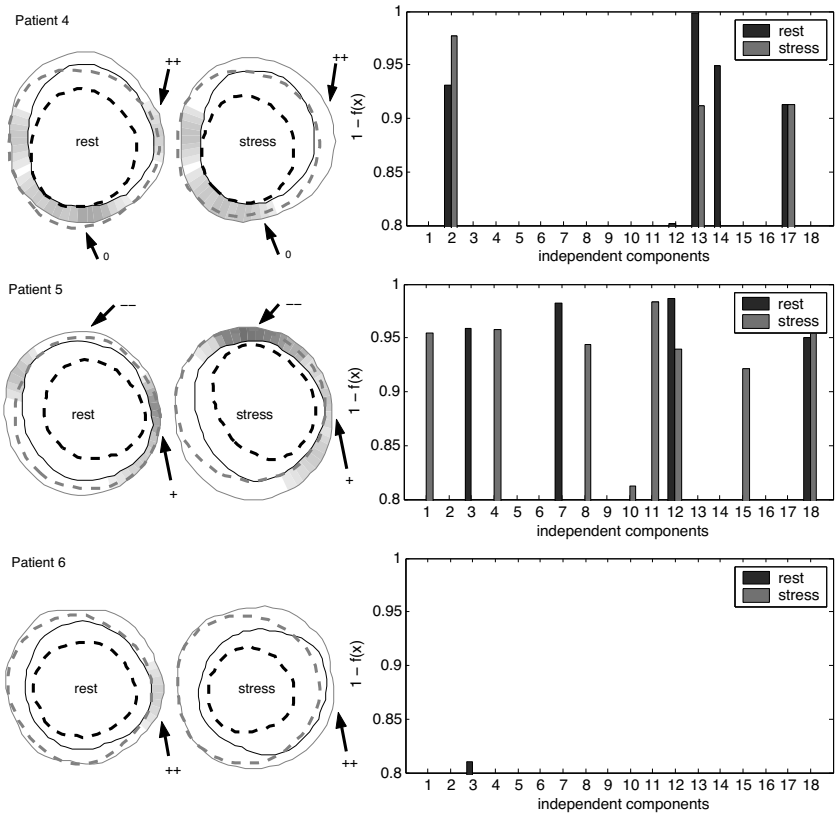


FIGURE 5.6: Qualitative prediction results of myocardial contractility improvement from Patients 4, 5, and 6. The leftmost and middle figures are quantification of abnormal regions from rest and stress respectively. ED and ES contours are drawn in solid and dashed lines respectively, to visualize contraction of the heart. The right most figure shows the abnormal independent components.

There is a case where an abnormal region does not improve its contractility in stress (Patient 4 with '0' sign) or even the contraction is getting worse in stress (Patient 5 with '–' sign). Another interesting case appears in Patient 2, where there is a region that has a small contraction in rest (see the arrow with 'D' sign), an improved contraction in stress, but abnormal motion in stress. This is detected by the model as an abnormal region.

## 5.3 Discussion

This chapter explores the potential of using ICA to model contraction of healthy hearts. The model is applied for detecting myocardial regions with abnormal contraction, both in rest and stress. Comparing the detection between rest and stress gives an indication of areas that may improve after treatment.

In Figure 5.5 and Figure 5.6, six examples of the prediction results using the ICA model are demonstrated. These examples show that the method is capable to perform comparative morphometrics between rest and stress. Abnormal myocardial regions in rest with decreasing probability value in stress are identified as viable but dysfunctional myocardium. These are regions that may gain improvement after treatment.

The detected abnormal regions both in rest and stress correspond visually with the lack of contractility on those regions (see Figure 5.5 and Figure 5.6). The method can also detect an abnormal motion in stress, even with increased contraction. This is possible, because the model is statistically trained from normal cardiac contraction, all deviations from normal contraction or motion are labeled as abnormal.

The current validation is still lack of gold standard data. The gold standard for the assessment of ischaemic heart disease is post-treatment data when it comes to the question whether myocardium improves or not after treatment. A proper validation for an automated contractility improvement assessment should utilize these data set.

To gain more accurate prediction of contractility improvement for the whole heart, extending the ICA model into a 3D model is necessary to detect abnormal myocardial segments [21]. This involves inclusion of three levels of short-axis MRI (apical, middle and basal) and one segment from vertical long axis.

## 5.4 References


[1] S. R. Underwood, J. J. Bax, J. vom Dahl, M. Y. Henein, J. Knuuti, A. C. van Rossum, E. R. Schwarz, J.-L. Vanoverschelde, E. E. van der Wall, W. Wijns, and Study Group of the European Society of Cardiology, "Imaging techniques for the assessment of myocardial hibernation. Report of a Study Group of the European Society of Cardiology," *Eur Heart J*, vol. 25, no. 10, pp. 815–36, May 2004.

[2] E. E. van der Wall, H. W. Vliegen, A. de Roos, and A. V. Bruschke, "Magnetic resonance imaging in coronary artery disease," *Circulation*, vol. 92, no. 9, pp. 2723–39, Nov 1995.

[3] R. J. van der Geest and J. H. Reiber, "Quantification in cardiac mri," *J Magn Reson Imaging*, vol. 10, no. 5, pp. 602–8, Nov 1999.

[4] E. Nagel and E. Fleck, "Functional MRI in ischemic heart disease based on detection of contraction abnormalities," *J Magn Reson Imaging*, vol. 10, no. 3, pp. 411–7, Sep 1999.

[5] F. M. Baer, E. Voth, P. Theissen, H. Schicha, and U. Sechtem, "Gradient-echo magnetic resonance imaging during incremental dobutamine infusion for the localization of coronary artery stenoses," *Eur Heart J*, vol. 15, no. 2, pp. 218–25, Feb 1994.

[6] A. Suinesiaputra, M. Üzümcü, A. F. Frangi, T. A. M. Kaandorp, J. H. C. Reiber, and B. P. F. Lelieveldt, "Detecting regional abnormal cardiac contraction in short-axis MR images using

independent component analysis," in *Medical Image Computing and Computer-Assisted Intervention – MICCAI 2004, Proceedings, Part I*, ser. Lecture Notes in Computer Science, C. Barillot, D. R. Haynor, and P. Hellier, Eds., vol. 3216. Springer, 2004, pp. 737–744.

[7] A. Hyvärinen, J. Karhunen, and E. Oja, *Independent Component Analysis*. John Wiley & Sons, Inc., 2001.

[8] S. Akaho, "Conditionally independent component analysis for supervised feature extraction," *Neurocomputing*, vol. 49, no. 1-4, pp. 139–150, 2002.

[9] M. S. Bartlett, J. R. Movellan, and T. J. Sejnowski, "Face recognition by independent component analysis," *IEEE Trans. on Neural Network*, vol. 13, no. 6, pp. 1450–1464, November 2002.

[10] T.-W. Lee and M. S. Lewicki, "Unsupervised image classification, segmentation, and enhancement using ICA mixture models," *IEEE Transactions on Image Processing*, vol. 11, no. 3, pp. 270–279, 2002.

[11] A. Hyvärinen, "Survey on independent component analysis," *Neural Computing Surveys*, vol. 2, pp. 94–128, 1999.

[12] I. L. Dryden and K. V. Mardia, *Statistical Shape Analysis*. John Wiley & Sons, 2002.

[13] F. P. van Rugge, E. E. van der Wall, S. J. Spanjersberg, A. de Roos, N. A. Matheijssen, A. H. Zwinderman, P. R. van Dijkman, J. H. Reiber, and A. V. Bruschke, "Magnetic resonance imaging during dobutamine stress for detection and localization of coronary artery disease. Quantitative wall motion analysis using a modification of the centerline method," *Circulation*, vol. 90, no. 1, pp. 127–38, Jul 1994.

[14] H. Stögbauer, R. G. Andrzejak, A. Kraskov, and P. Grassberger, "Reliability of ICA estimates with mutual information," in *Independent Component Analysis and Blind Signal Separation Proceedings*, ser. Lecture Notes in Computer Science, C. G. Puntonet and A. Prieto, Eds., vol. 3195. Springer, 2004, pp. 209–216.

[15] A. Cichocki, J. Karhunen, W. Kasprzak, and R. Vigário, "Neural networks for blind separation with unknown number of sources," *Neurocomputing*, vol. 24, no. 1-3, pp. 55–93, 1999.

[16] S. J. Roberts, "Independent component analysis: Source assessment & separation, a Bayesian approach," *IEEE Proceedings - Vision, Image & Signal Processing*, vol. 3, no. 145, pp. 149–154, 1998.

[17] J. Himberg, A. Hyvärinen, and F. Esposito, "Validating the independent components of neuroimaging time series via clustering and visualization," *Neuroimage*, vol. 22, no. 3, pp. 1214–22, Jul 2004.

[18] M. Bressan and J. Vitrià, "Independent modes of variation in point distribution models," in *Visual Form 2001 Proceedings*, ser. Lecture Notes in Computer Science, C. Arcelli, L. P. Cordella, and G. S. di Baja, Eds., no. 2059. Springer, 2001, pp. 123–134.

[19] B. Silverman, *Density Estimation for Statistics and Data Analysis*, ser. Monographs on Statistics and Applied Probability. London: Chapman and Hall, 1986.

[20] M. Wand and M. C. Jones, *Kernel Smoothing*. Chapman and Hall, 1995.

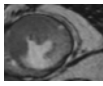

[21] M. D. Cerqueira, N. J. Weissman, V. Dilsizian, A. K. Jacobs, S. Kaul, W. K. Laskey, D. J. Pennell, J. A. Rumberger, T. Ryan, M. S. Verani, and American Heart Association Writing Group on Myocardial Segmentation and Registration for Cardiac Imaging, "Standardized myocardial segmentation and nomenclature for tomographic imaging of the heart: a statement for healthcare professionals from the Cardiac Imaging Committee of the Council on Clinical Cardiology of the American Heart Association," *Circulation*, vol. 105, no. 4, pp. 539–42, Jan 2002.